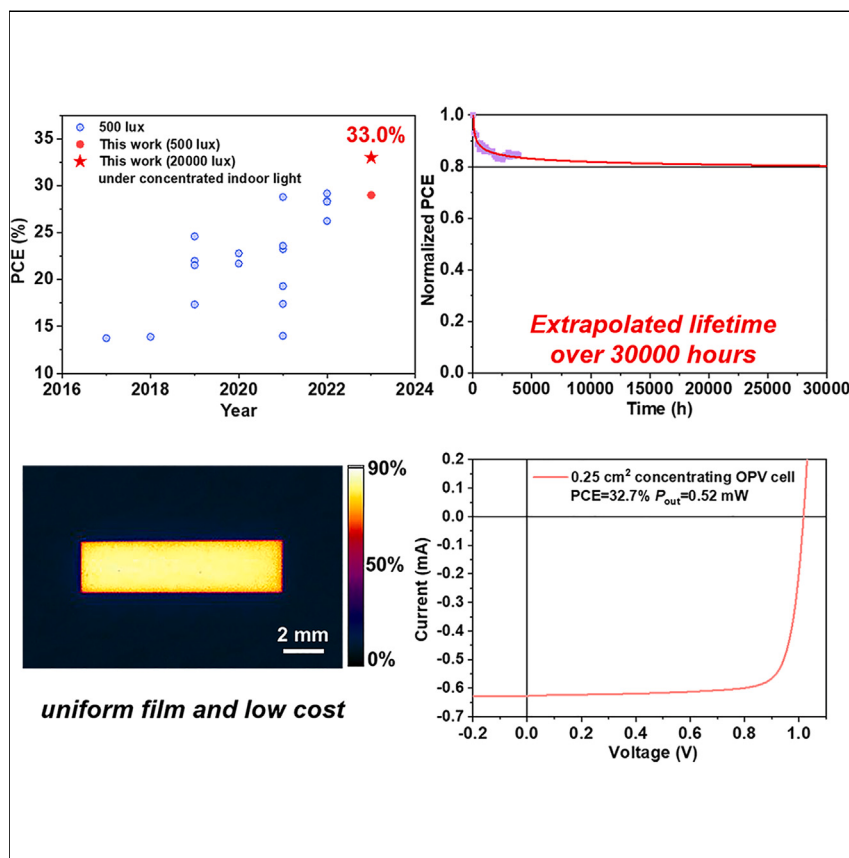


Article

High-performance organic photovoltaic cells under indoor lighting enabled by suppressing energetic disorders



In this work, we investigate the photovoltaic characteristics of organic photovoltaic (OPV) cells under concentrated indoor light. We demonstrate that concentrated indoor light is favorable for obtaining higher power conversion efficiency and maintaining excellent stability in OPV cells. We also confirm that a 0.25 cm² cell with a more uniform film under concentrated indoor light gives a higher output power than a 10 cm² cell at 500 lux, revealing that concentrating OPV cells have the potential for practical applications under indoor lighting.

Wenxuan Wang, Yong Cui, Tao Zhang, ..., Jingwen Wang, Shaoqing Zhang, Jianhui Hou

ycui1990@iccas.ac.cn

Highlights

The photovoltaic characteristics of the OPV cells under concentrated indoor light

An efficiency of 33% was achieved under concentrated indoor light

OPV cells with an extrapolated T₈₀ over 30,000 h under concentrated indoor light



Article

High-performance organic photovoltaic cells under indoor lighting enabled by suppressing energetic disorders

Wenxuan Wang,^{1,2} Yong Cui,^{1,4,*} Tao Zhang,^{1,2} Pengqing Bi,¹ Jianqiu Wang,¹ Shiwei Yang,³ Jingwen Wang,^{1,2} Shaoqing Zhang,³ and Jianhui Hou^{1,2,3}

SUMMARY

Organic photovoltaic (OPV) cells have exhibited great advantages for indoor applications. However, large energetic disorder restricts the performance of OPV cells under low illuminance, which brings significant challenges for indoor applications. Here, we demonstrate that concentrated indoor light can suppress the effects of energetic disorder and simultaneously enhance the open-circuit voltage and fill factor of OPV cells. Remarkably, PB2:FCC-Cl-based cells achieve a state-of-the-art PCE of 33.0% when concentrating indoor light to 20,000 lux. Meanwhile, all OPV cells exhibit superior stability under concentrated indoor light due to mild lighting conditions. Especially for the PBDB-TF:Y6 system exhibiting the best morphological stability, an extrapolated intrinsic lifetime is over 30,000 h. Combined with optical waveguide concentrators, we also reveal that concentrating OPV cells have the potential for low-cost manufacturing. These results suggest that developing concentrating OPV cells is quite necessary for indoor applications in the future.

INTRODUCTION

Organic photovoltaic (OPV) cells have prominent features such as light weight, flexibility, and tunable absorption spectrum, fully exploiting their potential for self-powered Internet of Things devices under indoor lighting.^{1–5} In the past few years, power conversion efficiencies (PCEs) of OPV cells have significantly increased with the development of wide-gap acceptors.^{6–9} Recently, Zhang et al. synthesized a wide-gap acceptor FTCC-Br and the OPV cells based on PB2:FTCC-Br achieved a record PCE of 30.2% under the LED (3,000 K) condition at 1,000 lux.⁸ However, this result is still significantly lower than the predicted PCE limit of over 40%.¹⁰ As previous research has suggested, organic semiconductors have larger energetic disorders than inorganic crystalline semiconductors, resulting in a broader distribution of density of states (DOS) in OPV cells.^{11–13} Under low light intensity, the broader DOS distribution invariably pushes photogenerated excitons further into tail states where energy levels of the trap state exist (Figure 1A); this causes a decreased splitting of the electron and hole quasi-Fermi levels (E_{Fn} and E_{Fp}) and reduces effective energy gap, actually decreasing the open-circuit voltage (V_{OC}).^{14–17} On the other hand, excitons limited by band-tail states can be easily quenched through Shockley-Read-Hall recombination, resulting in a larger voltage loss.¹⁸ Hence, it is essential to suppress the effects of energetic disorder on OPV cells for indoor applications, thereby improving the performance of OPV cells.

CONTEXT & SCALE

Organic photovoltaic (OPV) cells have prominent advantages such as light weight, flexibility, and tunable absorption spectra, exhibiting significant prospects for indoor applications. However, as organic semiconductors show large energetic disorder, the performance of the OPV cells is restricted under weaker illumination. Increasing light intensity by concentrating light for indoor OPV cells is an effective and direct strategy to suppress the effects of the energetic disorder. Here, we investigated the photovoltaic characteristics of the OPV cells under concentrated indoor light. The PB2:FCC-Cl-based cell achieved an efficiency of 33% under concentrated indoor light. Moreover, we demonstrated superior stability of the OPV cells with an extrapolated T_{80} over 30,000 h under indoor lighting. The application potential of the concentrating OPV cells is also investigated regarding the fabrication process.



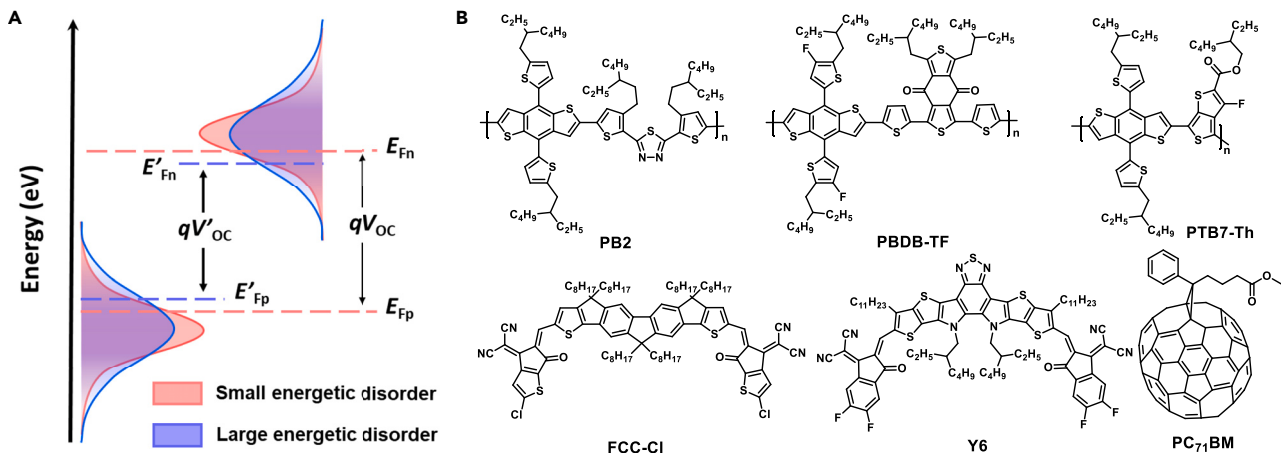


Figure 1. The schematic of DOS distribution and the chemical structures of the materials

(A) The schematic of DOS distribution.
(B) Chemical structures of the materials in this work.

Currently, designing materials with small energetic disorders is treated as the primary method. Previously, donors, PTBT-T¹⁹ and PTQ10,²⁰ and acceptors, Y11,¹² GS-ISO,⁶ 2BTP-2F-T,²¹ NITI,²² etc., are reported to suppress the energetic disorder of material systems and contribute to lower voltage losses. However, molecular design strategies meeting the requirements for indoor OPV cells are still lagging, and the broadening of DOS distribution has not been fundamentally solved in OPV cells. The V_{OC} decreases with reduced light intensity, bringing a significant challenge for the indoor applications of OPV cells.^{23–25} According to the international standard (lighting of indoor workplaces, CIE S 008/E-2001), the illuminance of buildings is generally in the range of 200–500 lux and most luminous environments of smart homes are even less than 100 lux, in which the V_{OC} will decrease more obviously. To suppress the effects of energetic disorder under weak ambient illumination, increasing light power density by concentrating light for OPV cells is a more effective and direct strategy. Although the development of concentrating technology has made great progress,^{26–30} the study of the effects of concentrated light on OPV cells is lacking under indoor lighting.

Herein, we investigated the effects of concentrated light on the characteristics of OPV cells and developed the application of concentrating OPV cells under indoor lighting. Three typical OPV systems (PBDB-TF:Y6, PB2:FCC-Cl, and PTB7-Th:PC₇₁BM, as shown in Figure 1B) are used as study subjects. We find these material systems present different energetic disorders and densities of trap states. Under low light intensity, larger energetic disorders evidently lead to severe trap-assist recombination. Nevertheless, the influence of energetic disorder can be largely suppressed under concentrated indoor light. Remarkably, the cell based on PB2:FCC-Cl yields a high PCE of 29.0% at 500 lux, whereas the PCE achieves an outstanding 33.0% when concentrating light to 20,000 lux, which is the highest PCE of OPV cells under indoor lighting, as we know. Meanwhile, three concentrating OPV cells exhibit superior stability under indoor light compared with the simulated sunlight. Benefiting from excellent morphological stability, the cells based on PBDB-TF:Y6 can maintain long-term stability with an extrapolated T_{80} (the time required to reach 80% of the initial PCE) of over 30,000 h under concentrated indoor light. Moreover, 0.25 cm² concentrating OPV cells prepared by the blade-coating method show more uniform films and a higher PCE than 10 cm² cells at 500 lux. Our work

¹Beijing National Laboratory for Molecular Sciences, CAS Research/Education Center for Excellence in Molecular Sciences, Institute of Chemistry, Chinese Academy of Sciences, Beijing 100190, P.R. China

²University of Chinese Academy of Sciences, Beijing 100049, P.R. China

³School of Chemistry and Biology Engineering, University of Science and Technology Beijing, Beijing 100083, P.R. China

⁴Lead contact

*Correspondence: ycui1990@iccas.ac.cn

<https://doi.org/10.1016/j.joule.2023.04.003>

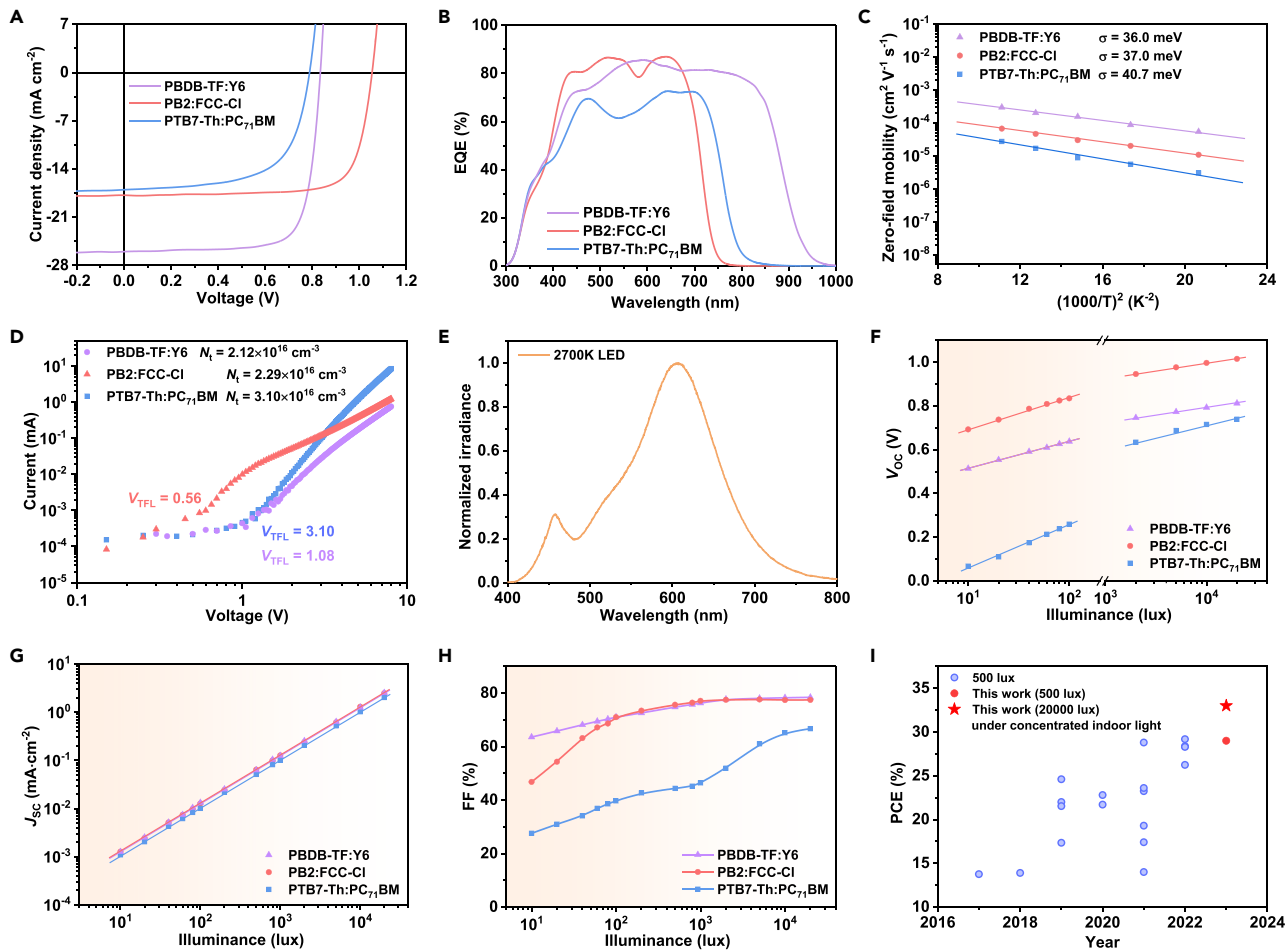


Figure 2. Photovoltaic characteristics of the OPV cells in this work

- (A) J-V curves of optimal OPV cells based on PBDB-TF:Y6, PB2:FCC-Cl, and PTB7-Th:PC₇₁BM under one sun.
- (B) The EQE curves of the three OPV cells.
- (C) Hole mobilities at different temperatures as a linear function of $1/T^2$ using temperature-dependent SCLC.
- (D) I-V curves of the corresponding electron-only devices.
- (E) The emission spectrum of adopted LED (2,700 K).
- (F–H) (F) V_{OC} , (G) J_{SC} , and (H) fill factor (FF) dependence on illuminance from 20,000 to 10 lux.
- (I) The development of the PCE of OPV cells at 500 lux. Red circle is the PCE value of PB2:FCC-Cl-based OPV cells under 500 lux in this work. Red star is the PCE obtained under concentrated indoor light with an illuminance concentrated to 20,000 lux, whereas the ambient illuminance is at about 500 lux indoors.

demonstrates that the concentrating OPV cells possess considerable potential for indoor applications.

RESULTS AND DISCUSSION

The OPV cells are fabricated with the structure of ITO/PEDOT:PSS/active layer/PDINN/Ag. First, we measured the device performance under AM 1.5 G simulated sunlight. The cells based on PBDB-TF:Y6, PB2:FCC-Cl, and PTB7-Th:PC₇₁BM obtain PCEs of 16.8%, 14.4%, and 8.58%, respectively. The current density-voltage (J-V) characteristics of the best cells are shown in Figure 2A, and the photovoltaic parameters are summarized in Table 1. Figure 2B depicts the external quantum efficiency (EQE) curves of the three OPV cells. The corresponding integrated current densities are 25.5, 17.1, and 16.2 mA cm^{-2} within 5% deviations of J_{SC} s. The above results are consistent with those of previous research.^{8,31,32}

Table 1. Detailed photovoltaic parameters of OPV cells under indoor light and AM 1.5G

Active layer	Light intensity	V _{OC} (V)	J _{SC} (mA cm ⁻²)	J _{cal} (mA cm ⁻²) ^a	FF (%)	PCE (%) ^b
PBDB-TF:Y6	500 lux LED	0.700	0.0629	0.0618	74.8	20.9 (20.2 ± 0.44)
	20,000 lux LED	0.812	2.54	2.47	78.4	25.6 (25.0 ± 0.60)
	AM 1.5G	0.839	26.0	25.5	76.9	16.8 (16.56 ± 0.18)
PB2:FCC-Cl	500 lux LED	0.909	0.0638	0.0601	78.9	29.0 (27.7 ± 0.53)
	20,000 lux LED	1.02	2.53	2.41	80.5	33.0 (32.0 ± 0.50)
	AM 1.5G	1.06	17.6	17.1	77.0	14.4 (14.1 ± 0.18)
PTB7-Th:PC ₇₁ BM	500 lux LED	0.470	0.0522	0.0504	37.5	5.84 (5.70 ± 0.23)
	20,000 lux LED	0.734	2.06	2.02	66.7	16.0 (15.8 ± 0.19)
	AM 1.5G	0.795	17.0	16.2	63.5	8.58 (8.35 ± 0.14)

^aJ_{cal} is the calculated J_{SC} by integrating the EQE spectrum over the light source.

^bThe average PCE values with standard deviations in parentheses are obtained from 8 individual cells.

To evaluate the energetic disorder, we first measured the Urbach energy (E_U) of OPV cells, which is positively related to the energetic disorder.^{33,34} By fitting the absorption tail of the highly sensitive EQE spectra (Figure S1A), the E_{Us} of PBDB-TF:Y6-, PB2:FCC-Cl-, and PTB7-Th:PC₇₁BM-based cells are calculated as 25.9, 26.3, and 35.5 meV respectively, implying an order of energetic disorder: PBDB-TF:Y6-based cells < PB2:FCC-Cl-based cells < PTB7-Th:PC₇₁BM-based cells. To verify the above result, we further evaluated the energetic disorder of the three systems via temperature-dependent space charge-limited current (SCLC) measurements. As shown in Figures 2C and S1B, the hole and electron energetic disorders (σ) are calculated using the Equation 1:

$$\mu_0 = \mu_\infty \exp \left[- \left(\frac{2\sigma}{3kT} \right)^2 \right] \quad (\text{Equation 1})$$

where μ_0 is zero-field mobility, μ_∞ is the mobility at infinite temperature, k is Boltzmann constant, and T is Kelvin temperature. Both the electron and the hole μ_0 of the three systems are shown as a linear function of $1/T^2$. The calculated hole energetic disorders for PBDB-TF:Y6-, PB2:FCC-Cl-, and PTB7-Th:PC₇₁BM-based devices display an increasing trend from 36.0 to 37.0, to 40.7 meV. Likewise, the electron energetic disorder also reveals an identical variation trend. These results indicate that the PTB7-Th:PC₇₁BM-based cell has much broader tails of DOS than the PBDB-TF:Y6- and PB2:FCC-Cl-based cells. In general, the energetic disorder is partly attributed to trap states existing in tail states.^{14,24} Therefore, we calculated the density of trap states (N_t) by SCLC measurements (Figure 2D). PBDB-TF:Y6-, PB2:FCC-Cl-, and PTB7-Th:PC₇₁BM-based devices show an incremental N_t of 2.12×10^{16} , 2.29×10^{16} , and 3.10×10^{16} cm⁻³, respectively, which proves the deeper traps in the tail states of the higher energetic disorder system. Moreover, the impedance measurements were carried out to verify the trend of N_t s. As shown in Figures S1C and S1D, the N_t s extracted from C⁻² versus V curves increase from PBDB-TF:Y6 (1.66×10^{23} m⁻³) to PB2:FCC-Cl (2.03×10^{23} m⁻³) and PTB7-Th:PC₇₁BM (2.28×10^{23} m⁻³), which is consistent with the results from the SCLC method.

We further measured the electroluminescence EQE (EQE_{EL}) for PBDB-TF:Y6-, PB2:FCC-Cl-, and PTB7-Th:PC₇1BM-based cells to evaluate the non-radiative voltage losses under low illuminance (Figure S2). From the EQE_{EL} curves, reasonable non-radiative voltage losses can be obtained when the current density in curves is equal to the J_{SC} of corresponding OPV cells under illumination.^{35,36} Therefore, the J_{SC} of OPV cells under low illuminance corresponds to the low current density region of EQE_{EL} curves. At this region, the three cells show decreasing EQE_{EL} values with different trends. This reveals a higher non-radiative voltage loss under low illuminance. As the illuminance decreases, PTB7-Th:PC₇1BM-based cells first exhibit a decreasing EQE_{EL} due to the highest energetic disorder, followed by PB2:FCC-Cl. By contrast, the PBDB-TF:Y6-based cell shows a decreasing EQE_{EL} value only at extremely low J_{SC} due to the lower energetic disorder and density of trap states. The results indicate that the additional voltage loss under low illuminance is related to non-radiative voltage loss.

To investigate the effects of concentrated indoor light on device performance, we measured the photovoltaic characteristics (V_{OC} , J_{SC} , FF, and PCE) under indoor light and concentrated indoor light. The emission spectra of the LED and the plot of irradiance versus illuminance are provided in Figures 2E and S3, respectively. Meanwhile, the uncertainty of the spectrometer and the homogeneity factor from the LED source are described in Table S1 and Figure S4, respectively, to give more detailed measurement information. For the intensity-dependent characteristics, the parameters of the three cells present different trends with decreasing illuminance. The V_{OC} versus illuminance shows two regions below 500 lux and above 2,000 lux with different slopes in terms of nkT/q (Figure 2F), where n is the diode ideality factor and q is the elementary charge. When the illuminance is above 2,000 lux, the slopes of PBDB-TF:Y6-, PB2:FCC-Cl-, and PTB7-Th:PC₇1BM-based cells are 1.11kT/q, 1.16kT/q, and 1.76kT/q, respectively, indicating relatively low trap-assist recombination at high illuminance,³⁷ and the V_{OC} s of corresponding cells are 0.812, 1.02, and 0.734 V, respectively, at 20,000 lux. However, the slopes of PBDB-TF:Y6-, PB2:FCC-Cl-, and PTB7-Th:PC₇1BM-based cells increase to 2.08kT/q, 2.38kT/q, and 3.22kT/q below 500 lux, which suggests severe trap-assist recombination at low illuminance. Especially for PTB7-Th:PC₇1BM-based cells with the largest density of trap states, the V_{OC} dramatically decreases to 0.068 V at 10 lux. Meanwhile, PBDB-TF:Y6-based cells have the smallest V_{OC} decrease due to the smallest density of trap states. In Figure 2G, the J_{SC} versus illuminance keeps an unchanged slope, close to 1, in a wide illuminance scale ranging from 20,000 to 10 lux, implying a negligible influence of energetic disorder on bimolecular recombination.²³ For FF, different decrease trends are also observed in the three cells under low illuminance (Figure 2H). The PBDB-TF:Y6-, PB2:FCC-Cl-, and PTB7-Th:PC₇1BM-based cells present FF of 63.6%, 46.8%, and 27.6% at 10 lux, respectively. Notably, the three cells show high and stationary FFs under high illuminance, close to the values under one sun. Based on the above three parameters, the cells based on PBDB-TF:Y6, PB2:FCC-Cl, and PTB7-Th:PC₇1BM obtain only 13.1%, 13.7%, and 0.3% PCEs at 10 lux, respectively (Figure S5). When the illuminance value reached 500 lux, the PCEs of the corresponding cells increased to 20.9%, 27.3%, and 5.84%, respectively. Excitingly, the PCEs of PBDB-TF:Y6 and PTB7-Th:PC₇1BM achieve reasonable values of 25.6% and 16.0% when concentrating light to 20,000 lux. More remarkably, the device based on PB2:FCC-Cl achieves an outstanding PCE of 33.0% at 20,000 lux and the corresponding output power density reaches 2.08 mW cm⁻², which is obviously higher than that of the state-of-the-art OPV cells as we know (Figure 2I; Table S2). The optimal photovoltaic parameters of three cells at 500 lux and 20,000 lux are summarized in Table 1. By the guide to the expression of uncertainty in

measurement (GUM) methods,³⁸ the PCE uncertainties based on the temporal and spatial uncertainties of the light source and the spectrometric uncertainty are calculated as 0.408% at 500 lux and 0.465% at 20,000 lux (Table S3). These results demonstrate that the large energetic disorder causes significantly low V_{OC} and FF under low illuminance, whereas concentrated light can effectively suppress the effects of energetic disorder on charge recombination and improve photovoltaic performance. Especially for material systems with a large energetic disorder, concentrated light is more beneficial to give reasonable V_{OC} and FF under weak illumination. By contrast, we also measured the device performance under concentrated sunlight, which was rarely studied before. As the light intensity is enhanced, the carrier density increases greatly. Therefore, the cells show extremely low FF (~45%) and PCE (5%–10%) (Table S4) due to excessive bimolecular recombination, suggesting that concentrated sunlight is adverse to device performance.

Furthermore, we measured the stability of the OPV cells under concentrated light and non-concentrated light. The cells were encapsulated by using normal glass with epoxy adhesive to block water and oxygen. As shown in Figures 3A, 3B, and S6, the OPV cells present superior stability under indoor lighting compared with one sun. After being exposed to continuous indoor light at 500 lux for 1,000 h, the cells based on PBDB-TF:Y6, PB2:FCC-Cl, and PTB7-Th:PC₇1BM can retain 80%, 82%, and 87% of their original PCEs, respectively (Figure 3A). When exposed to a concentrated indoor light of 20,000 lux, the cells display comparable stability after 1,000 h, indicating that concentrated indoor light has no distinct effect on device stability. By contrast, we also measured the device stability under one sun and concentrated sunlight. Under one sun, all cells show a quick decay within 24 h and maintain 73% (PBDB-TF:Y6), 50% (PB2:FCC-Cl), and 27% (PTB7-Th:PC₇1BM) (Figure 3B) of their original PCEs. Under concentrated sunlight, PB2:FCC-Cl-based cell suffers from severe decay and retains only about 10% of the original PCE. PTB7-Th:PC₇1BM-based cells also show a rapidly decreased PCE under concentrated sunlight compared with one sun. By contrast, the stability of PBDB-TF:Y6-based cells has no apparent difference under one sun and concentrated sunlight, and the decreases of the photovoltaic parameters are also less than those of PB2:FCC-Cl and PTB7-Th:PC₇1BM.

To explore the reasons for the difference in device stability under concentrated light, we first measured the ultraviolet-visible absorption spectrum variations of three blend films irradiated by concentrated sunlight in the N₂ glove box. As shown in Figures 3C–3E, the main absorption peaks of the PBDB-TF:Y6 film show little change, whereas the PB2:FCC-Cl and PTB7-Th:PC₇1BM films show a visible reduction. To further determine whether the strong solar radiation disrupts the molecular structure, the infrared spectra analysis of single material is performed under concentrated sunlight. As shown in Figures 3F, 3G, and S7, the infrared spectra of all the films show negligible changes after continuous radiation, which indicates unchanged chemical structures. As a result, the ultraviolet-visible absorption spectrum variation is likely attributed to the morphology change. The solar spectrum has a wider spectral range than indoor light (Figure S8). This implies the chemical structure will not change when the materials are exposed to indoor light. Infrared radiation presents a similar frequency to the intrinsic vibration frequency of molecules, contributing to molecule motion and collision. Consequentially, the infrared emission will dominate the thermal effect. The morphology behavior may be affected by the device temperature.^{39–42} Therefore, we measured the surface temperatures of the cells by thermal infrared imaging under different illumination. As indoor light has no infrared content, when the cells are continuously exposed to indoor light and concentrated indoor light for 30 min, the surface temperature can stay around the

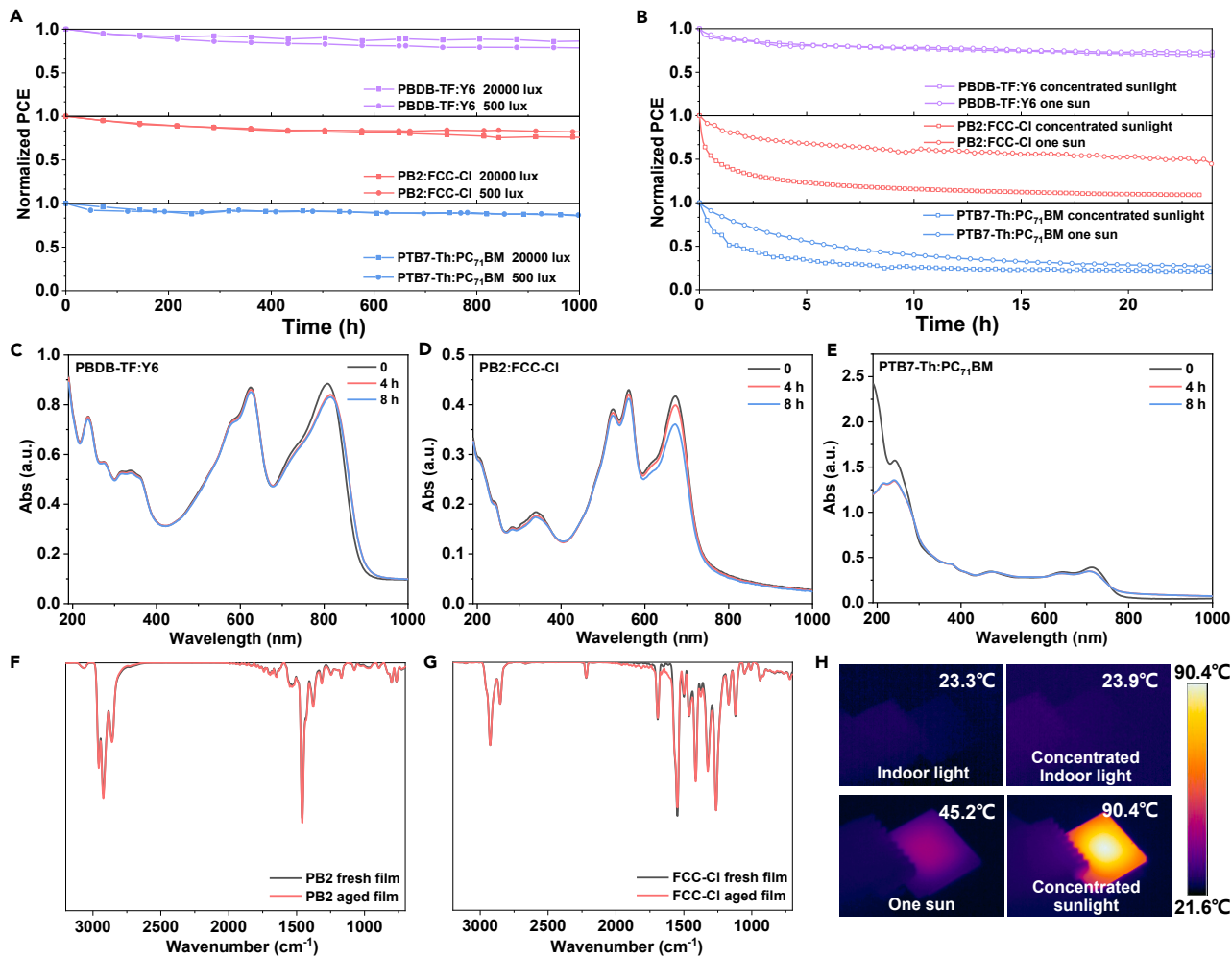


Figure 3. The stability measurements of the OPV cells and materials

(A) The device stability of PBDB-TF:Y6, PB2:FCC-Cl, and PTB7-Th:PC₇:BM at 500 lux indoor light (solid circle) and 20,000 lux concentrated indoor light (solid square).

(B) The device stability of PBDB-TF:Y6, PB2:FCC-Cl, and PTB7-Th:PC₇:BM under one sun (hollow circle) and concentrated sunlight (hollow square).

(C-E) The UV-vis spectra of (C) PBDB-TF:Y6, (D) PB2:FCC-Cl, and (E) PTB7-Th:PC₇:BM exposed in concentrated sunlight.

(F and G) The infrared spectra of fresh films and aged films of (F) PB2 and (G) FCC-Cl, respectively.

(H) The thermal infrared imaging of cell exposed in indoor light (left top), concentrated indoor light (right top), one sun (left bottom), and concentrated sunlight (right bottom).

ambient temperature (Figure 3H). Under one sun, however, the surface temperature rises to 45.2°C and even reaches a surprising 90.4°C under concentrated sunlight.

To investigate the morphology of the films, we conducted atomic force microscopy (AFM) measurements (Figures 4 and S9). We find that the morphology of all the aged films under continuous illumination of concentrated indoor light for 1,000 h is similar to that of the fresh films. It is obvious from the height images that all films possess uniform and smooth surfaces with root-mean-square roughness (R_q) of about 1.15 nm. In the phase images, the aged films show only slightly increased phase separation and domain size. Therefore, the OPV cells have excellent stability under concentrated indoor light. By contrast, the aged films exposed to concentrated sunlight deliver a significantly different morphology. The aged film based on PB2:FCC-Cl shows excessive miscibility between PB2 and FCC-Cl, leading to a significantly

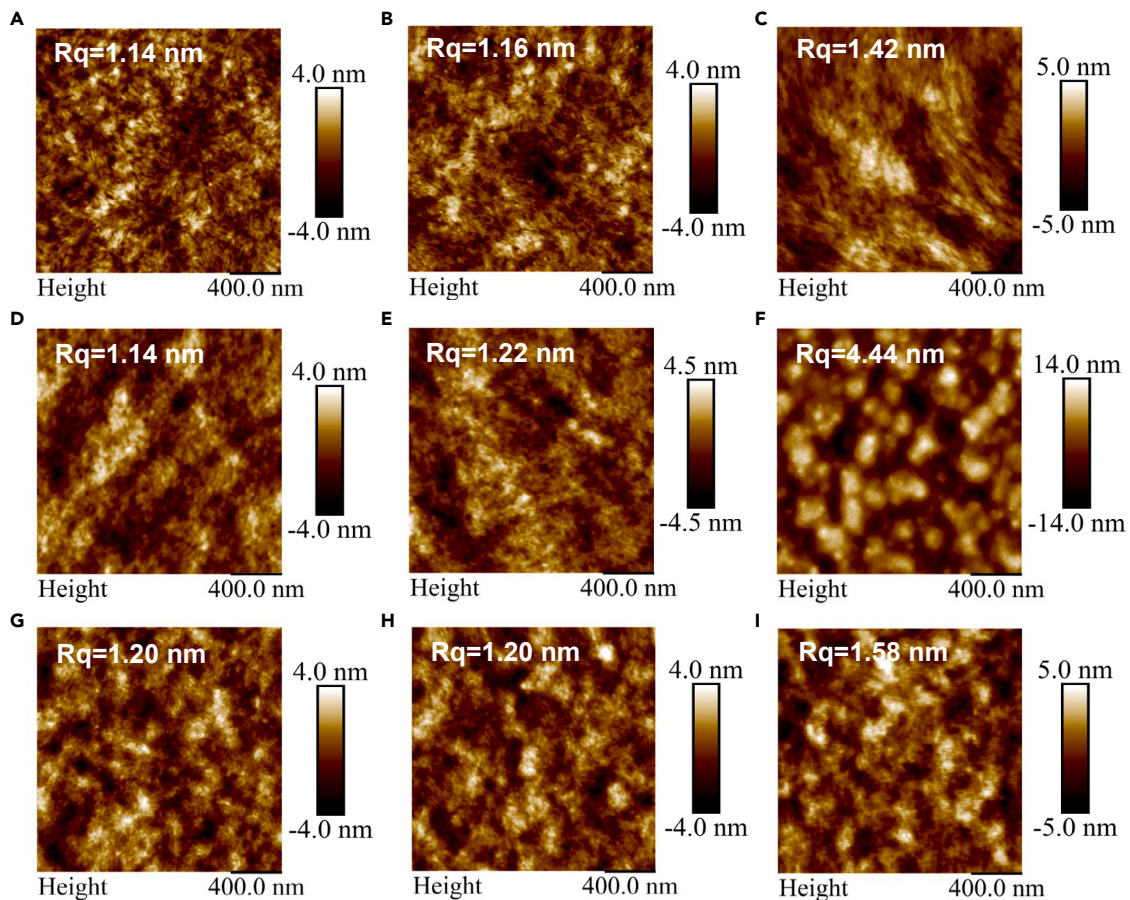


Figure 4. The morphology analysis of the active layers via AFM measurements

(A–C) The AFM height images of the fresh PB2:FCC-Cl film, PB2:FCC-Cl aged by concentrated indoor light, and concentrated sunlight.

(D–F) The AFM height images of the fresh PTB7-Th:PC₇₁BM film, and PTB7-Th:PC₇₁BM aged by concentrated indoor light and concentrated sunlight. (G–I) The AFM height images of the fresh PBDB-TF:Y6 film, PBDB-TF:Y6 aged by concentrated indoor light and concentrated sunlight. All processes are carried out in the N₂ glove box.

reduced degree of molecular aggregation than that exposed to concentrated indoor light. For the aged film based on PTB7-Th:PC₇₁BM, we can observe severe aggregation and phase separation in the phase images; meanwhile, the R_q of the film markedly increases to 4.44 nm. Notably, although exposed to concentrated sunlight, the PBDB-TF:Y6 film displays a homogeneous surface morphology with slightly increased phase separation. As a result, both the cells based on PB2:FCC-Cl and PTB7-Th:PC₇₁BM give significantly reduced PCEs under continuous illumination of the concentrated sunlight for 24 h, whereas the cells based on PBDB-TF:Y6 can maintain a higher value. We further determined the Flory-Huggins interaction parameter (χ) of PBDB-TF:Y6, PB2:FCC-Cl, and PTB7-Th:PC₇₁BM via contact angle measurements (Figure S10), in which the χ values are calculated via $(\sqrt{\gamma_{donor}} - \sqrt{\gamma_{acceptor}})^2$. A large χ value indicates low miscibility between the donor and the acceptor, which causes a trend of aggregation and large phase separation. By contrast, a small χ value presents a trend of excessive miscibility. Compared with PBDB-TF:Y6 with a χ value of 0.643, PTB7-Th:PC₇₁BM shows the largest χ value of 0.862, whereas PB2:FCC-Cl shows the smallest χ value of 0.341 (Table S5), which reveal the reason for different morphology behaviors of corresponding aged films under concentrated sunlight. As the PBDB-TF:Y6 film possesses the

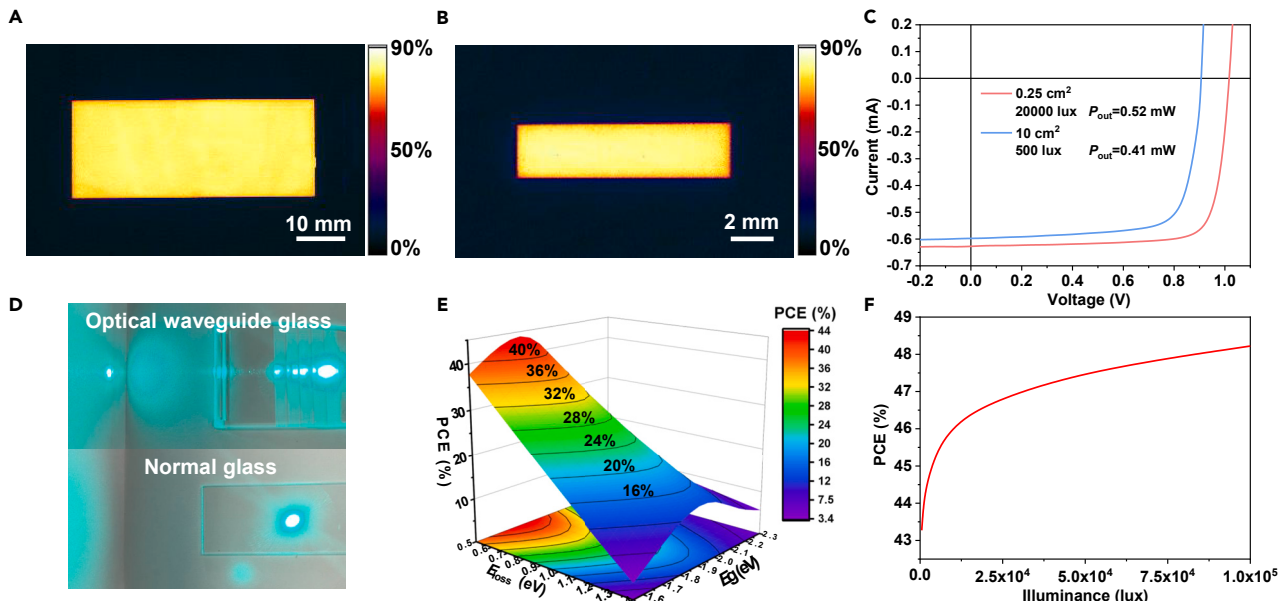


Figure 5. The prospects analysis of the concentrating OPV cells

(A and B) The EQE mapping of (A) 10 cm^2 and (B) 0.25 cm^2 blade-coated cells.

(C) I - V curves of the optimal cells with 10 and 0.25 cm^2 . The effective area of 10 cm^2 cell is 9.5 cm^2 .

(D) The real photographs of an optical waveguide glass (top) and normal glass (bottom) using a cyan laser to exhibit the optical path.

(E) The PCE prediction of OPV cells under indoor light (2,700 K, LED).

(F) The PCE prediction under concentrated indoor light in the illuminance range of 1,000–100,000 lux.

best morphological stability, we continue to track the stability of the PBDB-TF:Y6-based cell under concentrated indoor lighting (20,000 lux). As shown in Figure S11, the PCE of PBDB-TF:Y6-based cell almost maintained constant PCE from 1,000 to 4,000 h and the extrapolated T_{80} is over 30,000 h.

We investigate the applicability of concentrating OPV cells in terms of the fabrication process and production cost. In theory, the output power (P_{out}) of the 10 cm^2 OPV cell enables many styles of low-power consumption devices to be self-sustaining under indoor lighting of 500 lux. When the illuminance reaches 20,000 lux by concentrating indoor light, the cell area can be compressed to about 0.25 cm^2 to obtain a considerable P_{out} . To investigate their applicability in practically relevant technology, we employed the blade-coating method to fabricate 10 and 0.25 cm^2 cells based on high-performance PB2:FCC-Cl. As shown in Figures 5A and 5B, we measured the EQE mappings of the two cells. As it is difficult to control the deposition process for blade-coating large-area cells, such as casting temperature, the spacing between the blade and the substrate, the horizontality of the blade, and the effects of the solvent fluid dynamics,^{43,44} 0.25 cm^2 cell has a much more uniform film than the 10 cm^2 cell. The optimal current-voltage (I - V) curves of the two cells are plotted in Figure 5C. The 10 cm^2 cell yields a maximum PCE of 27.6% with a V_{OC} of 0.907 V, a J_{SC} of $62.9\text{ }\mu\text{A cm}^{-2}$, and a FF of 76.2% at 500 lux, and the corresponding P_{out} is 0.41 mW. Excitingly, the 0.25 cm^2 cell under concentrated light obtains a remarkably high PCE of 32.7% with improved V_{OC} (1.02 V), J_{SC} (2.53 mA cm^{-2}), and FF (80.6%). The P_{out} of the 0.25 cm^2 cell (0.52 mW) under concentrated indoor light is 26.8% higher than that of the 10 cm^2 cell at 500 lux.

Furthermore, we estimated the potential cost of the concentrating OPV cell and the large-area cell. Among various concentrators, an optical waveguide concentrator is

a promising technique that has the potential for concentrating indoor OPV cells.^{27–29} Figure 5D shows the real photographs of a planar grating optical waveguide (also known as a diffractive waveguide), in which a cyan laser is utilized to exhibit the optical path of optical waveguide glass. The incident light enters the optical waveguide glass and part of the light is reflected and exits from its sides. Figure S12 shows the spectrum of the reflected light, which is similar to the incident light. When a stripe-like OPV cell is attached to the side of the optical waveguide glass (Figure S13), the incident light power density can be controlled by designing an optical path in optical waveguide glass. According to previous literature, the price of an optical waveguide concentrator to increase the light power density for 0.25 cm² cell by 40 times is only about \$0.097.²⁶ Based on optical waveguide concentrators, the total cost of each concentrating OPV cell is only 0.24\$, which is much cheaper than the 10 cm² cell and is expected to decrease further in the future. The detailed cost is shown in Table S6. These results indicate that the concentrating OPV cells are easy to manufacture and have the potential for low-cost indoor applications. For example, the optical waveguide concentrating OPV cells can be used on electronic screens of Internet of Things products, such as electronic shelf labels and visual doorbells, showing potential market value. Nowadays, the optical waveguide has been successfully applied in virtual reality and augmented reality, although applying optical waveguides in indoor photovoltaic cells is still lacking. To achieve higher concentration performance, the optical paths of optical waveguide concentrators require a complex design. Thus, further developments of optical waveguides are necessary to realize the practical applications of the concentrating OPV cells.

Finally, we predict the PCE limit of OPV cells under concentrated indoor light. The ideal FF is estimated by the empirical relationship of FF and V_{OC} (Note S1, supplemental information).^{10,45} The upper limit of J_{SC} is integrated with a full-spectrum EQE of 85.0%. The ideal V_{OC} is calculated by $E_g - E_{loss}$. With the above assumptions, the PCE limit of around 43.3% is expected at 500 lux (2,700 K LED) when E_g is 1.8 eV and E_{loss} is as low as 0.5 eV (Figure 5E). Notably, when the illuminance increases to 100,000 lux by concentrating light, the PCE limit can break through to 48.2% (Figure 5F).

Conclusions

We study the applications of OPV cells under concentrated indoor light. We find that a larger energetic disorder causes severe trap-assist recombination under low illuminance, rapidly decreasing V_{OC} and FF. Nevertheless, concentrated indoor light can effectively suppress the effects of energetic disorder on charge recombination. For PTB7-Th:PC_{7,1}BM systems with a large energetic disorder, the PCE of the cell is significantly enhanced from 0.3% to 16% under concentrated indoor light. Noteworthily, the cell based on PB2:FCC-Cl achieves an outstanding PCE of 33.0%, which is the highest value of OPV cells for indoor applications. In addition, the indoor OPV cells show superiority in long-term stability due to mild conditions. The PBDB-TF:Y6-based cell with the most stable morphology presents an extrapolated T₈₀ of over 30,000 h. More importantly, we demonstrate that concentrating OPV cells have the potential for low-cost manufacturing. Based on the blade-coating method, the 0.25 cm² concentrating cell has a much more uniform film and higher PCE than the 10 cm² cell. Then, we confirm that the 0.25 cm² cell under concentrated indoor light gives an approximately 27% higher P_{out} than the 10 cm² cell at 500 lux. These results demonstrate developing concentrating OPV cells offers a practical prospect for indoor applications.

EXPERIMENTAL PROCEDURES

Resource availability

Lead contact

Further information and requests for resources and materials should be directed to and will be fulfilled by the lead contact, Y.C. (ycui1990@iccas.ac.cn)

Materials availability

This study did not generate new unique materials.

Data and code availability

The published article includes all data generated or analyzed during this study.

Full experimental procedures are provided in the supplemental information.

SUPPLEMENTAL INFORMATION

Supplemental information can be found online at <https://doi.org/10.1016/j.joule.2023.04.003>.

ACKNOWLEDGMENTS

This work was financially supported by the National Natural Science Foundation of China (nos. 52003275, 52120105005, and 22275195). J.H. was supported by the Key Research Program of the Chinese Academy of Sciences, grant no. XDPB13. Thank Lingxi-AR Technology Co., Ltd. for providing optical waveguide glass.

AUTHOR CONTRIBUTIONS

W.W., Y.C., and J.H. conceived the idea and designed the study. W.W., Y.C., and T.Z. fabricated the photovoltaic cells and carried out the published device data measurements. W.W. and S.Y. provided the thermal infrared imaging data. P.B. and J.W. measured temperature-dependent SCLC. W.W. and T.Z. performed the AFM measurements. J.W. synthesized the donor material PB2. Y.C., S.Z., and J.H. contributed to the data interpretation. W.W., Y.C., and J.H. wrote the paper. All the authors discussed the results and commented on the manuscript.

DECLARATION OF INTERESTS

The authors declare no competing interests.

Received: September 16, 2022

Revised: October 24, 2022

Accepted: April 5, 2023

Published: April 27, 2023

REFERENCES

1. Xie, L., Song, W., Ge, J., Tang, B., Zhang, X., Wu, T., and Ge, Z. (2021). Recent progress of organic photovoltaics for indoor energy harvesting. *Nano Energy* 82, 105770. <https://doi.org/10.1016/j.nanoen.2021.105770>.
2. Mainville, M., and Leclerc, M. (2020). Recent progress on indoor organic photovoltaics: from Molecular Design to production scale. *ACS Energy Lett.* 5, 1186–1197. <https://doi.org/10.1021/acsenergylett.0c00177>.
3. Cui, Y., Hong, L., and Hou, J. (2020). Organic photovoltaic cells for indoor applications: opportunities and challenges. *ACS Appl. Mater. Interfaces* 12, 38815–38828. <https://doi.org/10.1021/acsami.0c10444>.
4. Ryu, H.S., Park, S.Y., Lee, T.H., Kim, J.Y., and Woo, H.Y. (2020). Recent progress in indoor organic photovoltaics. *Nanoscale* 12, 5792–5804. <https://doi.org/10.1039/d0nr00816h>.
5. Cui, Y., Xu, Y., and Hou, J. (2022). High efficiency and more functions bring a bright future for organic photovoltaic cells. *Sci. Bull.* 67, 1300–1303. <https://doi.org/10.1016/j.scib.2022.05.015>.
6. Bi, P., Zhang, S., Ren, J., Chen, Z., Zheng, Z., Cui, Y., Wang, J., Wang, S., Zhang, T., Li, J., et al. (2022). A high-performance nonfused wide-bandgap acceptor for versatile photovoltaic applications. *Adv. Mater.* 34, e2108090. <https://doi.org/10.1002/adma.202108090>.
7. Bai, F., Zhang, J., Zeng, A., Zhao, H., Duan, K., Yu, H., Cheng, K., Chai, G., Chen, Y., Liang, J., et al. (2021). A highly crystalline non-fullerene acceptor enabling efficient indoor organic photovoltaics with high EQE and fill factor. *Joule* 5,

- 1231–1245. <https://doi.org/10.1016/j.joule.2021.03.020>.
8. Zhang, T., An, C., Xu, Y., Bi, P., Chen, Z., Wang, J., Yang, N., Yang, Y., Xu, B., Yao, H., et al. (2022). A medium-bandgap nonfullerene acceptor enabling organic photovoltaic cells with 30% efficiency under indoor artificial light. *Adv. Mater.* 34, e2207009. <https://doi.org/10.1002/adma.202207009>.
9. Ding, Z., Zhao, R., Yu, Y., and Liu, J. (2019). All-polymer indoor photovoltaics with high open-circuit voltage. *J. Mater. Chem. A* 7, 26533–26539. <https://doi.org/10.1039/C9TA10040G>.
10. Cui, Y., Wang, Y., Bergqvist, J., Yao, H., Xu, Y., Gao, B., Yang, C., Zhang, S., Inganäs, O., Gao, F., and Hou, J. (2019). Wide-gap non-fullerene acceptor enabling high-performance organic photovoltaic cells for indoor applications. *Nat. Energy* 4, 768–775. <https://doi.org/10.1038/s41560-019-0448-5>.
11. Yuan, J., Zhang, C., Qiu, B., Liu, W., So, S.K., Mainville, M., Leclerc, M., Shoaei, S., Neher, D., and Zou, Y. (2022). Effects of energetic disorder in bulk heterojunction organic solar cells. *Energy Environ. Sci.* 15, 2806–2818. <https://doi.org/10.1039/D2EE00271J>.
12. Liu, S., Yuan, J., Deng, W.Y., Luo, M., Xie, Y., Liang, Q.B., Zou, Y.P., He, Z.C., Wu, H.B., and Cao, Y. (2020). High-efficiency organic solar cells with low non-radiative recombination loss and low energetic disorder. *Nat. Photonics* 14, 300–305. <https://doi.org/10.1038/s41566-019-0573-5>.
13. Shuttle, C.G., Treat, N.D., Douglas, J.D., Fréchet, J.M.J., and Chabinyc, M.L. (2012). Deep energetic trap states in organic photovoltaic devices. *Adv. Energy Mater.* 2, 111–119. <https://doi.org/10.1002/aenm.201100541>.
14. Blakesley, J.C., and Neher, D. (2011). Relationship between energetic disorder and open-circuit voltage in bulk heterojunction organic solar cells. *Phys. Rev. B* 84, 075210. <https://doi.org/10.1103/PhysRevB.84.075210>.
15. Hood, S., Zarrabi, N., Meredith, P., Kassal, I., and Armin, A. (2019). Measuring energetic disorder in organic semiconductors using the photogenerated charge-separation efficiency. *J. Phys. Chem. Lett.* 10, 3863–3870. <https://doi.org/10.1021/acs.jpclett.9b01304>.
16. Cui, Y., Yao, H.-F., Xu, Y., Bi, P.-Q., Zhang, J.-Q., Zhang, T., Hong, L., Chen, Z.-H., Wei, Z.-X., Hao, X.-T., and Hou, J.-H. (2022). 100 cm² organic photovoltaic cells with 23% efficiency under indoor illumination. *Chin. J. Polym. Sci.* 40, 979–988. <https://doi.org/10.1007/s10118-022-2761-x>.
17. Gao, F., Tress, W., Wang, J., and Inganäs, O. (2015). Temperature dependence of charge carrier generation in organic photovoltaics. *Phys. Rev. Lett.* 114, 128701. <https://doi.org/10.1103/PhysRevLett.114.128701>.
18. Li, L., Kwon, J.H., and Jang, J. (2012). Tail states recombination limit of the open circuit voltage in bulk heterojunction organic solar cells. *Org. Electron.* 13, 230–234. <https://doi.org/10.1016/j.orgel.2011.11.006>.
19. Bi, P., Ren, J., Zhang, S., Zhang, T., Xu, Y., Cui, Y., Qin, J., and Hou, J. (2021). Suppressing energetic disorder enables efficient indoor organic photovoltaic cells with a PTV derivative. *Front. Chem.* 9, 684241. <https://doi.org/10.3389/fchem.2021.684241>.
20. Sun, C., Pan, F., Bin, H., Zhang, J., Xue, L., Qiu, B., Wei, Z., Zhang, Z.G., and Li, Y. (2018). A low cost and high performance polymer donor material for polymer solar cells. *Nat. Commun.* 9, 743. <https://doi.org/10.1038/s41467-018-03207-x>.
21. Zhang, L., Zhang, Z., Deng, D., Zhou, H., Zhang, J., and Wei, Z. (2022). “N-pi-N” type oligomeric acceptor achieves an OPV efficiency of 18.19% with low energy loss and excellent stability. *Adv. Sci. (Weinh)* 9, e2202513. <https://doi.org/10.1002/advs.202202513>.
22. Zhou, Z., Xu, S., Song, J., Jin, Y., Yue, Q., Qian, Y., Liu, F., Zhang, F., and Zhu, X. (2018). High-efficiency small-molecule ternary solar cells with a hierarchical morphology enabled by synergizing fullerene and non-fullerene acceptors. *Nat. Energy* 3, 952–959. <https://doi.org/10.1038/s41560-018-0234-9>.
23. Hartnagel, P., and Kirchartz, T. (2020). Understanding the light-intensity dependence of the short-circuit current of organic solar cells. *Adv. Theor. Simul.* 3, 2000116. <https://doi.org/10.1002/adts.202000116>.
24. Chen, Z., Wang, T., Wen, Z., Lu, P., Qin, W., Yin, H., and Hao, X.-T. (2021). Trap state induced recombination effects on indoor organic photovoltaic cells. *ACS Energy Lett.* 6, 3203–3211. <https://doi.org/10.1021/acsenergylett.1c01336>.
25. Burwell, G., Sandberg, O.J., Li, W., Meredith, P., Carnie, M., and Armin, A. (2022). Scaling considerations for organic photovoltaics for indoor applications. *Sol. RRL* 6, 2200315. <https://doi.org/10.1002/solr.202200315>.
26. Kant, K., Nithyanandam, K., and Pitchumani, R. (2021). Analysis and optimization of a novel hexagonal waveguide concentrator for solar thermal applications. *Energies* 14, 2146. <https://doi.org/10.3390/en14082146>.
27. Currie, M.J., Mapel, J.K., Heidel, T.D., Goffri, S., and Baldo, M.A. (2008). High-efficiency organic solar concentrators for photovoltaics. *Science* 321, 226–228. <https://doi.org/10.1126/science.1158342>.
28. Wei, A.-C., Chen, Z.-R., and Sze, J.-R. (2016). Planar solar concentrator with a v-groove array for a side-absorption concentrated photovoltaic system. *Optik* 127, 10858–10867. <https://doi.org/10.1016/j.ijleo.2016.08.045>.
29. Elikkottil, A., Tahersima, M.H., Gupta, M.V.N.S., Maiti, R., Sorger, V.J., and Pesala, B. (2019). a spectrally tunable dielectric subwavelength grating based broadband planar light concentrator. *Sci. Rep.* 9, 11723. <https://doi.org/10.1038/s41598-019-48025-3>.
30. Ramachandran, A.M., S, S.M., Thampi, A.S., Singh, M., and Asok, A. (2022). A comprehensive review on optics and optical materials for planar waveguide-based compact concentrated solar photovoltaics. *Results Eng.* 16, 100665. <https://doi.org/10.1016/j.rineng.2022.100665>.
31. Yuan, J., Zhang, Y., Zhou, L., Zhang, G., Yip, H.-L., Lau, T.-K., Lu, X., Zhu, C., Peng, H., Johnson, P.A., et al. (2019). Single-junction organic solar cell with over 15% efficiency using fused-ring acceptor with electron-deficient core. *Front. Chem.* 9, 684241. <https://doi.org/10.3389/fchem.2021.684241>.
32. Liao, S.H., Jhuo, H.J., Cheng, Y.S., and Chen, S.A. (2013). Fullerene derivative-doped zinc oxide nanofilm as the cathode of inverted polymer solar cells with low-bandgap polymer (PTB7-Th) for high performance. *Adv. Mater.* 25, 4762–4771. <https://doi.org/10.1002/adma.201301476>.
33. Kaiser, C., Sandberg, O.J., Zarrabi, N., Li, W., Meredith, P., and Armin, A. (2021). A universal Urbach rule for disordered organic semiconductors. *Nat. Commun.* 12, 3988. <https://doi.org/10.1038/s41467-021-24202-9>.
34. Schopp, N., Luong, H.M., Luginbuhl, B.R., Panoy, P., Choi, D., Promarak, V., Brus, V.V., and Nguyen, T.-Q. (2022). Understanding interfacial recombination processes in narrow-band-gap organic solar cells. *ACS Energy Lett.* 7, 1626–1634. <https://doi.org/10.1021/acsenergylett.2c00502>.
35. Rau, U. (2007). Reciprocity relation between photovoltaic quantum efficiency and electroluminescent emission of solar cells. *Phys. Rev. B* 76, 085303. <https://doi.org/10.1103/PhysRevB.76.085303>.
36. Yao, J., Kirchartz, T., Vezie, M.S., Faist, M.A., Gong, W., He, Z., Wu, H., Troughton, J., Watson, T., Bryant, D., and Nelson, J. (2015). Quantifying losses in open-circuit voltage in solution-processable solar cells. *Phys. Rev. Appl.* 4, 014020. <https://doi.org/10.1103/PhysRevApplied.4.014020>.
37. Kuik, M., Koster, L.J., Wetzelra, G.A., and Blom, P.W. (2011). Trap-assisted recombination in disordered organic semiconductors. *Phys. Rev. Lett.* 107, 256805. <https://doi.org/10.1103/PhysRevLett.107.256805>.
38. Theodorou, D., Meligotsidou, L., Karavoltos, S., Burnetas, A., Dassenakis, M., and Scoullos, M. (2011). Comparison of ISO-GUM and Monte Carlo methods for the evaluation of measurement uncertainty: application to direct cadmium measurement in water by GFAAS. *Talanta* 83, 1568–1574. <https://doi.org/10.1016/j.talanta.2010.11.059>.
39. Yang, C., Zhan, S., Li, Q., Wu, Y., Jia, X., Li, C., Liu, K., Qu, S., Wang, Z., and Wang, Z. (2022). Systematic investigation on stability influence factors for organic solar cells. *Nano Energy* 98, 107299. <https://doi.org/10.1016/j.nanoen.2022.107299>.
40. Zhang, L., Zhao, H., Hu, M., Wang, X., Hu, L., Mao, H., Yuan, Z., Ma, W., and Chen, Y. (2021). Enhanced efficiency and excellent thermostability in organic photovoltaics via ternary strategy with twisted conjugated compound. *Small* 17, e2103537. <https://doi.org/10.1002/smll.202103537>.
41. Zhou, K., Xin, J., and Ma, W. (2019). Hierarchical morphology stability under multiple stresses in organic solar cells. *ACS Energy Lett.* 4, 447–455. <https://doi.org/10.1021/acsenergylett.8b02383>.
42. Yang, W., Luo, Z., Sun, R., Guo, J., Wang, T., Wu, Y., Wang, W., Guo, J., Wu, Q., Shi, M., et al. (2020). Simultaneous enhanced efficiency and

- thermal stability in organic solar cells from a polymer acceptor additive. *Nat. Commun.* 11, 1218. <https://doi.org/10.1038/s41467-020-14926-5>.
43. Xiao, Y., Zuo, C., Zhong, J.X., Wu, W.Q., Shen, L., and Ding, L. (2021). Large-area blade-coated solar cells: advances and perspectives. *Adv. Energy Mater.* 11, 2100378. <https://doi.org/10.1002/aenm.202100378>.
44. Gu, X., Shaw, L., Gu, K., Toney, M.F., and Bao, Z. (2018). The meniscus-guided deposition of semiconducting polymers. *Nat. Commun.* 9, 534. <https://doi.org/10.1038/s41467-018-02833-9>.
45. Green, M.A. (1981). Solar cell fill factors: general graph and empirical expressions. *Solid State Electron.* 24, 788–789. [https://doi.org/10.1016/0038-1101\(81\)90062-9](https://doi.org/10.1016/0038-1101(81)90062-9).